Numerical Modeling of GFRP Reinforced Concrete Slabs

Omer R EL Zaroug[1]   **John P Forth**[2]   **Jianqiao YE**[3]

1 Omar AL Mukhtar University || Al Bayda || Libya   2 Leeds University || Leeds || UK

3 Lancaster University || Lancaster || UK

Abstract: The use of non-metallic fibre reinforced polymer reinforcement as an alternative to steel reinforcement in concrete is gaining acceptance mainly due to its high corrosion resistance. High strength-to-weight ratio, high stiffness-to-weight ratio and ease of handling and fabrication are added advantages. Other benefits are that they do not influence to magnetic fields and radio frequencies and they are thermally non-conductive. However, the stress-strain relationship for Glass fibre reinforced polymer reinforcement (GFRP) is linear up to rupture when the ultimate strength is reached. Unlike steel reinforcing bars, GFRP rebars do not undergo yield deformation or strain hardening before rupture. Also, GFRP reinforcement possesses a relatively low elastic modulus of elasticity compared with that of steel. As a consequence, for GFRP reinforced sections, larger deflections and crack widths are expected than the ones obtained from equivalent steel reinforced sections for the same load. This investigation provides details of the numerical analysis of GFRP reinforced slabs loaded mechanically using the commercial finite element program (DIANA). To prove the validity of the proposed finite element approach, a comparison is made with experimental test results obtained from full-size slabs. The comparisons are made on the basis of first cracking load, load-deflection response at midspan, cracking patterns, mode of failure and loads at failure. Using the DIANA software for the analysis of GFRP reinforced slabs under mechanical load is possible and can produce acceptable predictions throughout the load range in terms of final load and crack patterns. However, DIANA overestimated the first cracking load and tended to over predict the experimental deflections.

Key words: Nonlinear analysis; FRP reinforced concrete; cracking; GFRP rods.

1. Introduction

The flexural design of concrete sections reinforced with Glass FRP is different from that of sections reinforced with steel because of the difference in mechanical properties of GFRP and steel. Generally, the GFRP bars used as reinforcement in concrete have tensile strengths varying between 620 and 690 MPa and a modulus of elasticity of around 40 GPa [1]. The tensile strength varies as the diameter of the bar increases due to shear lag which develops between the fibers in the larger sizes. The stress-strain relationship for GFRP is linear up to rupture when the ultimate strength is reached. Unlike steel reinforcing bars, GFRP rebars do not undergo yield deformation or strain hardening before rupture. For this reason, the flexural design of sections reinforced with GFRP has been based on: (i) ultimate strength, (ii) serviceability (the low elasticity modulus of GFRP shifts the design criteria to the serviceability limit states that check the structural behaviour aspect instead of the strength to assure functionality and safety during

its life), (iii) shear and (iv) deformability (the deformability factor is defined as the product ratio of moment multiplied by curvature at ultimate failure and at serviceability [2]. For steel reinforced sections, the cross section of steel is commonly governed by the ultimate strength requirement. There are, however, some cases where the design is governed by the need to control crack width in service (e.g. water retaining structures).

GFRP reinforced concrete members have a relatively low stiffness after cracking. Consequently, the permissible deflection under service loads can control the design. In general, designing GFRP reinforced cross sections for concrete crushing failure satisfies the serviceability criteria for deflection and crack width [2]. Deflections in ACI 440 [2] are calculated based on an effective second moment of area, I_e (Eq. 1).

However, Ospina and Nanni [3] stated that the term β_d (Eq. 2) which is dependent on ρ_{bf} is conceptually incorrect. This is because it would imply that different deflections can be predicted for members reinforced with FRP bars that have similar stiffness but different ultimate tensile strength, f_{fu}. Since deflection is a problem associated with the serviceability limit state, the procedure should not be linked to ultimate limit state parameters such as f_{fu}.

$$I_e = \left(\frac{M_{cr}}{M_a}\right)^3 \beta_d\, I_g + \left[1 - \left(\frac{M_{cr}}{M_a}\right)^3\right] I_{cr} \leq I_g \quad (1)$$

$$\beta_d = \frac{\rho_f}{5\,\rho_{fb}} \leq 1.0 \qquad (2)$$

A second observation noted by Bischoff [4] refers to the β_d definition. FRP-reinforced concrete beams and one-way slabs do not have reduced tension stiffening because of the FRP reinforcement properties but because of the tension-stiffening component in the original Branson's equation, which is very large for FRP-reinforced concrete members. At crack locations, the concrete carries essentially zero tension. Between cracks, however, the concrete participates in resisting tensile stress because of bond between the reinforcement and the concrete. This effect is often referred to as tension stiffening and is taken into account with the effective second moment of area [5].

On the other hand, researches based on an evaluation of experimental results from several studies have demonstrated that the degree of tension stiffening is affected by the amount and stiffness of the flexural reinforcement and by the relative reinforcement ratio (ratio of ρ_f to ρ_{fb}) [6 & 7].

The Nonlinear finite element (NLFE) model Using DIANA software [8] appears to be one of the options which can be used to predict load-deflection curves of GFRP reinforced concrete slabs. It can also be used to provide a valuable supplement to the laboratory investigations, in terms of further parametric studies. A major advantage of the NLFE model is that it can reduce the amount of experimental work and hence, reduce costs.

2. Experimental Program

Three concrete slabs were constructed and tested. The slabs had the same cross sectional dimensions, b = 500 mm and h = 150 mm "Fig. 1" with total length of 2800 mm. They were reinforced longitudinally using GFRP rebar of 12.7 mm nominal diameters (d_b). No stirrups were provided in the test specimens. The reinforcement ratio (ρ_f), the clear bar spacing (**cbs**) and GFRP arrangement were all varied "Table 1". The concrete cover (**c**) on both side of the specimens was kept constant (50 mm) in all test slabs. The slab specimens were simply supported with a span of 2400 mm and a shear span of 800 mm. All concrete specimens were subjected to two concentrated loads, each applied at one third of the 2400 mm tested length.

2.1 Materials Properties

Glass Fiber Reinforced Polymer rebar was selected because it is the most widely used in the composite industry. The GFRP rebars are made of continuous longitudinal E-glass fibers bound together with a vinylester resin matrix with an external sand coating [1]. The bars contained 70% fiber by volume. The longitudinal modulus of elasticity of GFRP, E_g is 40.8 GPa, and its ultimate strength, f_{fu} is 690 MPa for 12.7 mm bar diameters.

The concrete mix design had the following properties: a water-cement ratio of 0.55, 355 kg/m^3 pure Portland cement, 195 kg/m^3 water, 724 kg/m^3 fine aggregate and 1086 kg/m^3 quartzite aggregate (maximum 20 mm diameter). No super plasticizer was added to increase the concrete workability. Three concrete cubes (100 x 100 x 100 mm) were tested in compression at 28 days according to BS EN 12390-3:2000 [9], and three cylinders (150 mm diameter x 300 mm long) were also tested for splitting strength according to BS EN 12390-6:2000 [10].The maximum compressive strength of the concrete was 55 MPa (strength class C55/45) and the splitting strength ranged from 2.7 to 3.3 MPa.
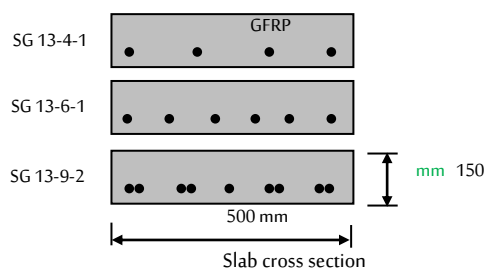
Fig. 1 Mechanical loading test set-up

Table 1 GFRP reinforcement in test Specimens

Slab specimens	No. of bars	d_b (mm)	ρ_f (%)	c (mm)	cbs (mm)	GFRP arrangement
SG13-4-1	4	12.7	0.82	20	116	Single bar
SG13-6-1	6	12.7	1.23	20	65	Single bar
SG13-9-2	9	12.7	1.84	25	72	Bundled bar

3. Description of the 3D NLFE Model

The reinforced concrete specimen of length 2800 mm, width 500 mm and height 150 mm was modeled as a three dimensional system. However, due to symmetry only the left half of the specimen and the loading scheme were modeled "Fig. 2". This approach significantly reduced the computational time and computer space requirement. In all the NLFE analyses, the concrete body was modeled using HX24L – brick element, 8 nodes. It is based on a linear interpolation and Gaussian integration. The element is capable of plastic deformation, cracking in three orthogonal directions and crushing. GFRP bars were modeled by a truss element embedded in the adjacent concrete mother element. Axial elongation was the only available deformation.

The smeared crack approach (i.e. it considers cracks as regions of damaged material with degraded properties) in combination with the plasticity model was selected to model the cracking and crushing of concrete due to its computational convenience as well as its resemblance to reality.
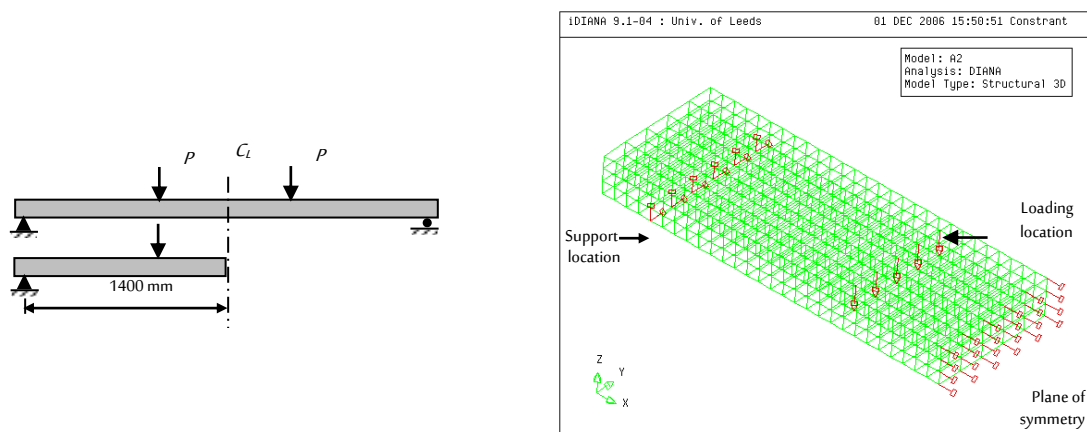
Fig. 2 NLFE model of GFRP rod embedded in concrete

4. Results and Discusions

4.1 First Cracking Load

Loads at first cracking from the experimental results and the model are compared in "Table 2". In all slabs, the first cracking load obtained from NLFE model was higher than the experimental data by about 13 to 50 %. The overestimation of first cracking load in the NLFE model is possibly due to:

- The relative homogeneity of the NLFE model may not compare to the relative homogeneity of an actual slab specimen, as the latter contains a number of micro cracks produced by drying and handling [11]. These cracks may reduce the stiffness of the actual slabs, whilst the NLFE models do not include micro-cracks.

- The tension-softening curve used in the NLFE analysis was a brittle cracking model in which the ultimate strain was fixed and always equal to fct/Ec.

Table 2 First cracking loads

Slab	f_{ct} (MPa)	First cracking load (kN)	
		Experiment	DIANA
SG13-4-1	2.7	13.0	15.0
SG13-6-1	3.3	12.0	18.5
SG13-9-2	3.2	14.0	18.5

4.2 Load-deflection Curves up to Ultimate Load

The load-deflection curves from both experimental and NLFE results are plotted in "Fig. 3". In the linear region, the NLFE results have similar trends to the test specimens up to 10 kN when the slab specimens start to crack, and become less stiff, as is evident in the "Fig. 3". However, the NLFE trend continues to increase linearly and cracks at a higher load than the loads from the experimental results "Table 2". Explanations for these higher cracking loads were provided in the previous section. At initial cracking, the NLFE model indicates a constant load even though the deflection continues to increase. One explanation for these increased deflections is the larger number of cracks found in the NLFE results than that observed in the test specimen.

It can be seen from "Fig. 3" that all NLFE models increase linearly in the secondary linear region up to the load before the final load. The NLFE model appeared to predict the behaviour of slab SG13-4-1 with ρ_f = 0.82% "Fig. 3a" throughout the range of post cracking up to a load of 75 kN reasonably well (within 2% to 13%). As Figure 3b shows, at a load below 55 kN the NLFE deflections overestimate (by a maximum of 48%) the experimental deflection of slab SG13-6-1 whereas at a load of 60 kN and above the model only underestimates the experimental data by a maximum of 7%. It can be seen from Figure 3C that at lower loads (i.e. 25 kN) the NLFE model over predicts the experimental deflection by 56% whereas at higher loads (i.e. 105 kN) it only underestimates the experimental data by 3%.

As shown by the results "Fig. 3", larger deflections begin to occur at a load just prior to the final load in the NLFE models and hence, the NLFE models give a clear indication of the ultimate load (large deflection before failure). In contrast, the test specimens failed suddenly without any warning (no large deflection as in the NLFE model).

It can be concluded that the deflections of GFRP slabs can generally be predicted by the NLFE analysis. However, the NLFE predictions are better for lower reinforcement ratios (i.e. < 1%).
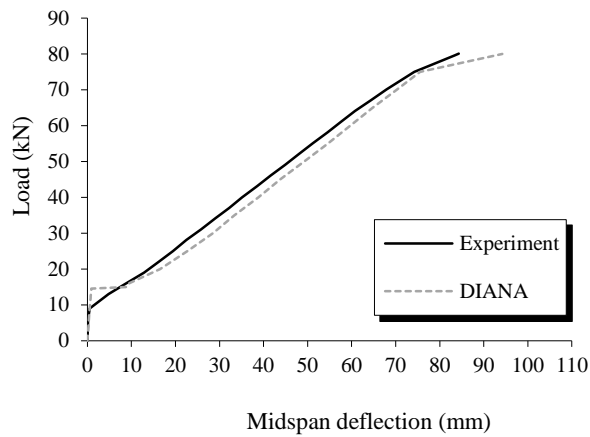
a) Slab SG13-4-1
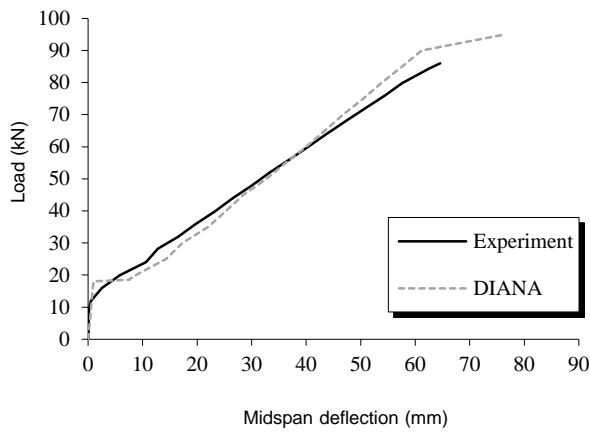
b) Slab SG13-6-1
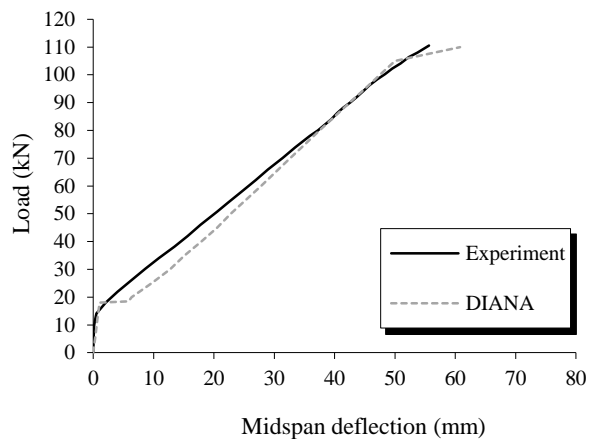
c) Slab SG13-9-2

Fig. 3 Load-deflection response for slabs

4.3 NLFE cracking patterns

Figures 4 and 5 show crack development in the slab models SG13-6-1 CS and SG13-9-2 at a load level of 80 kN (at about 93 and 73% of ultimate load, respectively) as in the experimental investigation. The NLFE crack patterns were very similar to that of the experimental crack patterns. In all slab models, the first crack occurred at different load levels within the constant moment zone. Flexural cracking consisting of vertical cracks perpendicular to the direction of the principal tensile stress occurred early at midspan.

As the load increased, the vertical flexural cracks spread horizontally from the midspan to the support. Cracking outside the constant moment zone (shear span of 800 mm on each side) started similarly to the flexural cracking. At a higher load, additional cracks started to form throughout the length of the specimen, propagating upward. In the last few load steps, compressive cracks started to occur at the top surface of the slab models. Finally, failures occurred by shear followed by concrete crushing at a maximum load. The cracking behaviour obtained from the FE models at the load levels before the final load correspond well with the observed crack patterns of the slab specimens.
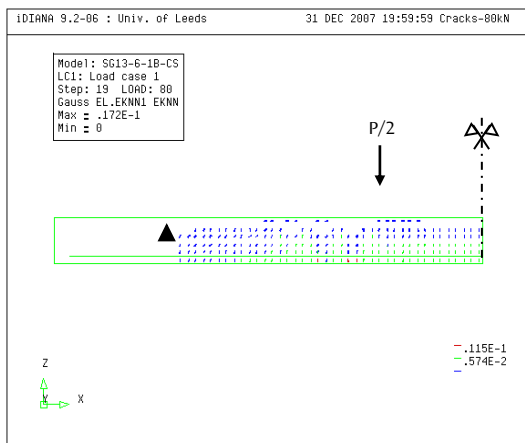
a) NLFE model cracks
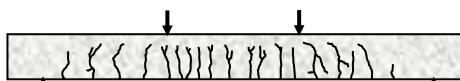
b) Experimental cracks

Fig. 4 Cracks for SG13-6-1 at 80 kN
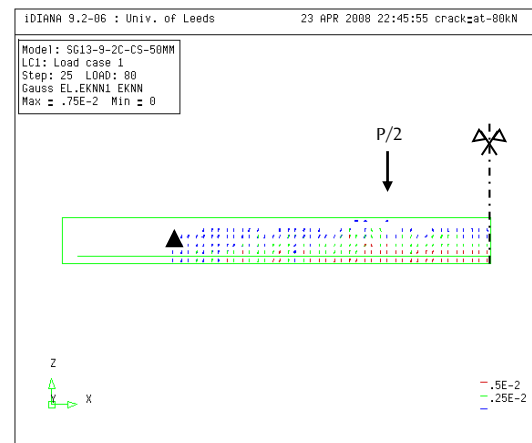
a) NLFE model cracks
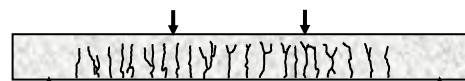
b) Experimental cracks

Fig. 5 Cracks for SG13-9-2 at 80 kN

4.4 Modes of Failure

A shear failure was observed in all control specimens followed by a compression failure at the top of the slab specimens. Crack patterns obtained from the finite element analysis at the last converged load steps are compared to the cracks at failure from the actual test slabs "Fig. 6". As shown in the figures, the crack patterns at failure from the NLFE model and the actual slab agree very well. Diagonal shear cracks

propagate from near the support toward the loading area. The cracks occurred mostly in the shear stress region.

In addition, numerous compressive cracks occurred at the top part of the slab. Many flexural cracks were observed at mid span as well. The crack patterns "Fig. 6" obtained from the NLFE model support the experimental results which suggest that the slabs failed in shear followed by concrete crushing. Although the slab models had a GFRP reinforcement ratio (ρ_f) above the balanced ratio (ρ_{fb}), this shear failure does not satisfy the failure mode predicted by ACI-440 [2] (when $\rho_f > \rho_{fb}$, concrete crushing governs). However, the shear failure mode was not surprising due to the absence of links in the shear spans.
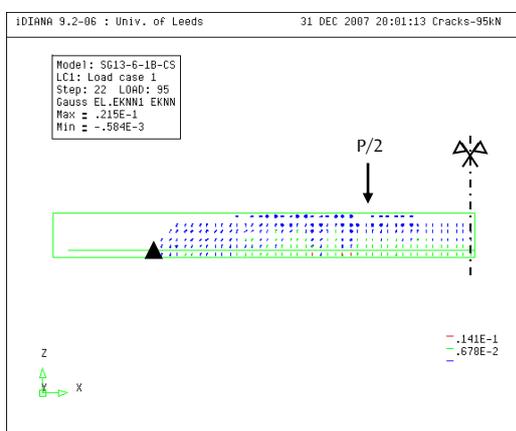
a) NLFE failure mode	b) Experimental failure mode

Fig. 6 Slab SG13-6-1at Failure

4.5 Loads at Failure

Table 3 compares the ultimate loads from the test slabs and the final loads from the finite element analysis. At the NLFE loads listed in Table 3, the slab models can no longer support additional load as indicated by the increasing deflection "Fig. 3" and severe cracking throughout the entire slab models is predicted "Fig. 6". The results in Table 3 Indicate that the final load predictions obtained from the finite element simulations were close to the ultimate loads of the experimental results.

Table 3 Comparison between Exp. & NLFE ultimate loads

Slab	Ultimate load (kN)		NLFE/Exp.
	Experiment	NLFE	
SG13-4-1	81	75	0.93
SG13-6-1	86	90	1.05
SG13-9-2	111	105	0.95

5. CONCLUSIONS

1. The first cracking load from the NLFE model was higher than that from the experimental data. This is mainly due to the reasons listed in first cracking load section.

2. The NLFE deflections "Fig. 3" at mid span over predicted the experimental deflections. DIANA is more accurate for models/slabs with lower reinforcement ratios (i.e. < 1%).

3. Final crack patterns are similar in appearance to the experimental slabs.

4. The crack patterns at failure "Fig. 6" obtained from the NLFE model also suggest that the slabs failed in shear followed by concrete crushing.

5. The results "Table 3" indicate that the final load predictions obtained from the NLFE analysis were close (within 5% to 8%) of the ultimate loads obtained from the experimental results. As shown by the results "Fig. 3" the NLFE model gives a clear indication of the ultimate load (large deflection before failure).

6. Using the DIANA software for the analysis of GFRP reinforced slabs under mechanical load is possible and can produce acceptable predictions throughout the load range in terms of final load and crack patterns.

References

1. Hughes Brothers, Inc. (2002). Aslan 100 Fiber glass Rebars. Technical Data: www.hughesbros.com.

2. ACI Committee 440 (ACI 440.1R-06), (2006). Guide for the Design and Construction of Structural Concrete Reinforced with FRP Bars. American Concrete Institute.

3. Ospina, C.E. and Nanni, A. (2007). Current FRP-Reinforced Concrete Design Trends in ACI 440.1R. In: the 8th international symposium on fiber-reinforced polymer reinforcement for concrete structures, FRPRCS-8. Patras, Greece, July 16-18, 2007.

4. Bischoff, P.H. (2007). Rational model for calculating deflection of reinforced concrete beams and slabs. Canadian Journal of Civil Engineering, 34 (8), pp. 992-1002.

5. Bischoff, P.H. and Scanlon, A. (2007). Effective moment of inertia for calculating deflections of concrete members containing steel reinforcement and fiber-reinforced polymer reinforcement. ACI Structural Journal, 104 (1), pp. 68-75.

6. Toutanji, H. and Saafi, M. (2000). Flexural Behavior of Concrete Beams Reinforced with Glass Fiber-Reinforced Polymer (GFRP) Bars. ACI Structural Journal , V. 97, No. 5, Sept.-Oct., pp. 712-719.

7. Yost, J., Gross, S., and Dinehart, D. (2003). Effective Moment of Inertia for GFRP Reinforced Concrete Beams. ACI Structural Journal, V. 100, No. 6, Nov.-Dec., pp. 732-739.

8. DIANA Finite Element Analysis, (2005). User's Manual Release 9. TNO DIANA BV. Delft, the Netherlands.

9. British Standards Institution. (2000). BS EN 12390-3: 2000. Testing hardened concrete, part 3: compressive strength of test specimens. London, British Standards Institution, pp.10.

10. British Standards Institution. (2000). BS EN 12390-6: 2000. Testing hardened concrete, part 6: tensile splitting strength of test specimens. London, British Standards Institution, pp.10.

11. Neville, A. M. (1996). Properties of Concrete. Fourth edition, Addison Wesley Longman Limited, Harlow, England.

Nomenclature:

I_e	Effective second moment of area (mm^4)
I_{cr}	Cracked second moment of area (mm^4)
I_g	Gross second moment of area (mm^4)
M_a	Applied moment (N mm)
M_{cr}	Cracking moment (N mm)
β_d	Reduction coefficient
ρ_f	FRP reinforcement ratio
ρ_{fb}	Balanced reinforcement ratio of FRP rods

الملخص: إن استخدام قضبان التسليح غير المعدنية المصنوعة من الالياف البوليمرية كبديل لقضبان حديد التسليح في الخرسانة يكتسب قبولا اكثر بسبب عدم قابليته للتآكل وتميزه بالمقاومه العالية وخفة الوزن وسهولة المناولة والتصنيع. هناك فوائد اخرى منها عدم تأثيره على المجالات المغناطيسية والترددات الراديوية وكذلك كونه غير موصل للحرارة. ومع ذلك ، فإن علاقة الإجهاد والانفعال لقضبان الالياف الزجاجية هي علاقة خطية وتستمر الى حمل الانهيار. وعلى العكس من قضبان حديد التسليح ، فان قضبان الالياف الزجاجية لاتمتلك خاصية الخضوع و معامل المرونة لها منخفض. ونتيجة لذلك ، فان الاعضاء الانشائية المسلحة بقضبان الالياف الزجاجية يحدث بها هبوط اكبر وعرض تشققات اكثر مقارنة بالاعضاء الانشائية المسلحة بقضبان حديد التسليح والمعرضة لنفس الاحمال. فى هذا البحث تم دراسة التحليل العددي للبلاطات المسلحة بقضبان الالياف الزجاجية تحت تأثير الاحمال الميكانيكية باستخدام برنامج ديانا للعناصر المحدودة (DIANA). ولإثبات صحة نتائج النموذج تمت مقارنة نتائج التحليل العددي مع النتائج المتحصل عليها معملياً لنفس ابعاد النموذج. تم إجراء المقارنات على أساس : الحمل عند ظهور أول تشقق ، علاقة الحمل بالهبوط عند المنتصف ، أنماط التشققات ، نوع الانهيار والحمل عند الانهيار. اظهرت النتائج امكانية استخدام برنامج ديانا لتحليل البلاطات تحت الحمل الميكانيكي وخاصةً علاقة الحمل بالهبوط و اقصى حمل وانماط التشققات ، ولكن نتائج الحمل عند ظهور أول تشقق كانت اعلى نسبياً عن النتائج المعملية.